Application of principal component analysis for improvement of X-ray fluorescence images obtained by polycapillary-based micro-XRF technique

AUTHOR(S):

Aida, S.; Matsuno, T.; Hasegawa, T.; Tsuji, K.

CITATION:

Aida, S. ...[et al]. Application of principal component analysis for improvement of X-ray fluorescence images obtained by polycapillary-based micro-XRF technique. Nuclear Instruments and Methods in Physics Research Section B: Beam Interactions with Materials and Atoms 2017, 402: 267-273

ISSUE DATE:

2017-07-01

URL:

http://hdl.handle.net/2433/226368

Application of principal component analysis for reproduction of X-ray fluorescence images with high quality

S. Aida*[a], T. Matsuno[a], T. Hasegawa[b], K. Tsuji[a]

[a] *Graduate School of Engineering, Osaka City University, 3-3-138, Sugimoto, Sumiyoshi, Osaka 558-8585, Japan*

[b] *Institute for Chemical Research, Kyoto University, Gokasho, Uji, Kyoto 661-0011, Japan*

ABSTRACT

Micro x-ray fluorescence (micro-XRF) analysis gives elemental maps by repeating EDS analysis in the interesting region. However, in some cases, the obtained XRF images of trace elements are not clear due to high background intensity. To solve this problem, we applied principal component analysis (PCA) to XRF spectra to reduce the background intensity. We focused on the improvement of quality of XRF imaging by applying the PCA. Standard deviations of XRF intensities in PCA-filtered image were

improved, leading to clear contrast of objective image on low background. Also, we confirmed that the spatial resolution in XRF images was improved by applying PCA. This improvement of XRF image was effective in the case where the XRF intensity was weak.

Keywords: micro-XRF, principal component analysis, elemental mapping, XRF imaging

1. Introduction

XRF analysis enables elemental analysis for various samples. By using the x-ray focusing lens, XRF analysis at the small region has been possible as well known as micro-XRF analysis [1, 2]. To know the elemental distributions, micro-XRF analysis is also applied as the sample is scanned [2]. ROI (range of interest) intensities in the x-ray spectra are registered at the corresponding position. Finally, we can get XRF images for the sample. However, when the concentration of analyzing elements is low, the created image is not clear due to relatively high background intensity. Therefore, the technique to reduce the background intensity is required. A total reflection XRF is one of such techniques. Also, the use of ultra-thin sample support for a small volume liquid sample

is useful for this purpose.

A principal component analysis (PCA) is well known statistical technique. PCA gives eigenvectors and score vectors for spectrum data set. That means that the spectrum data set is expressed as the product of the eigenvector and the corresponding score vector, The products showing a large contribution to data set are called as “principal components”. In the conventional approach, PCA is applied to bring out principal components and extract the important information from the original data [3, 4].

So far, PCA has been applied to XRF analysis of various samples. The researchers at University of Antwerp created principal component maps derived from XRF maps [3]. The researchers at the University of Manchester applied the PCA to the data obtained for hard X-ray imaging [4]. In addition, PCA has been used for Raman imaging by researchers at Advanced Industrial Science and Technology (AIST) [5]. Not only imaging method, PCA has been applied in various spectrometry methods as traditional statistic technique [6, 7].

The researchers at Argonne National Laboratory performed micro-XRF imaging for biological sample (cell and bacteria) [8]. By limiting the data set with principal and major components, they reduced the noise levels. Then, XRF spectrum was re-created with the components having large eigenvalues. Finally, elemental maps were also

re-created. They showed the advantage of eliminating the overlap with P-Kα from Au-Mα [8]. In the present paper, we focused on the improvement of quality of XRF images by applying PCA regarding the contrast of the XRF image and the spatial resolution.

2. Experimental setup

Figure 1 (a) shows the laboratory-made micro-XRF instrument using an x-ray polycapillary full lens (manufactured by X-ray Optical Systems, USA) combined with a fine-focused x-ray tube. The polycapillary lens gave an x-ray micro beam with a beam size of 10 μm at a focal distance of 2 mm. An x-ray tube with Mo anode (MCBM 50-0.6B, manufactured by rtw, Germany) was operated 50 kV and 0.5 mA. A silicon drift detector, (SDD, XR-100CR, manufactured by Amptek Inc., USA) was employed to detect x-rays. The detection area was 50 mm^2, and energy resolution was 130eV at Mn Kα. A spectrum was described by 2,048 channel, in energy range of 0-20 keV.

A small volume of the standard solution was dropped on a glass plate. The dried residues obtained from the 2.5 ppm solution of Fe and Cu are shown in Fig. 2. The sample was scanned with a step of 10 μm by using the x-y stage (YM05A-R1, Kohzu Precision Co. Ltd., Japan). XRF analysis was performed for 1 s or 10 s at each position.

XRF mapping was performed for an area of 500 μm x 500 μm.

3. Principal component analysis (PCA)

Since a sample area of 500 μm x 500 μm was analyzed with a step of 10 μm, 2,601 (= 51 x 51) spectra were totally obtained, as illustrated in Fig.3 (a). The spectra set were constructed in the order of coordinate ((1, 1), (1, 2), …, (51, 51)), which was defined as "matrix-A" (Fig.3 (b)). An XRF spectrum was composed of 2,048 energy channels in our experimental condition. Since 2,601 spectra were obtained, matrix-A was composed of 2,601 (columns) x 2,048(lines), as shown in Fig. 3 (b). A square matrix was created from data matrix-A and transposed matrix A^T, leading to eigenvalues and eigenvectors, as shown in Fig.3(c). The first eigenvector is expressed so that dispersion of the original data is smallest. Eigenvalues show how the corresponding eigenvector contributes to the original data. As shown in Fig. 3(d), the data matrix-A can be expressed with the following equation (1) using the eigenvectors (p) and score vectors (t) [9-12].

$$A = t_1 p_1 + t_2 p_2 + \cdots + t_n p_n \qquad (1)$$

The first principal component (t_1p_1) gives the largest contribution an approximation as to how an averaged spectrum for the whole data would look [8]. It is familiar approach that the parts of data are extracted by taking principal components [9]. Thus,

the raw data (matrix-A) were interpreted by adding all inner vectors of the eigenvector and the corresponding score vector. Figure 4 shows the contribution of the eigenvalues with different basic components. We can recognize that the first and second principal components showed a large contribution to total eigenvalues. This means XRF data can be expressed with these principal components. Thus, we considered that the components labeled with the number more than three were a kind of noise factors, leading to background intensities. A new spectra data, matrix-B was reconstructed using only principal components after eliminating small contribution. Therefore, the data matrix B is given by the equation (2):

$$\mathrm{B} = t_1 p_1 + t_2 p_2 \qquad (2)$$

Finally, we can re-cerate XRF spectrum using only principal components. Of course, we can make ROI for the obtained spectrum. Then, XRF maps could be re-constructed with small background.

4. Applying PCA for micro-XRF imaging

We measured Fe XRF images for the residue made from the Fe standard solution. Usually, XRF image is made from strong Fe Kα intensity. However, weak Kβ peak on a relatively large background was used for Fe map in order to investigate how PCA is

effective for reducing the background. Experimental Fe Kβ image is shown in Fig. 5 (a). As described, Fe Kβ image is not clear due to high background. PCA was applied for this data set. We can choose how many principal components should be included in new data matrix-B. Figures 5 (b)-(f) indicate the re-created images with different numbers of the components from 2 to 300. As the number is increased, the re-created image (shown in Fig. 5 (f)) approached to the original raw map (Fig. 5 (a)). In the present case, we considered that two principal components was the best to express the Fe distribution with good quality, as shown in Fig. 5 (b).

Figure 6 (a) shows Cu Kα image obtained for Cu residue with a measurement time of 1 s per pixel, while Figs.6 (c) and (e) were Cu Kβ images obtained with different measurement times of 1 s and 10 s per pixel, respectively. The XRF images in the right side (Figs.6 (b), (d) and (f)) were recreated from the data matix-B including PCA-filtered spectra. Similarly, two principal components were applied. As shown in Fig.6 (b), the PCA-filtered Cu Kα image was close to the original one (Fig.6 (a)). That means, PCA was not so effective in the case where the XRF intensity was strong and originally clear image was obtained. The raw Cu Kβ images shown in Figs.6 (c) and (e) were not so clear, because of the weak intensity and relative high background intensity. In these cases, the PCA-filtered XRF maps were clear compared to the original maps, as

shown in Figs. 6 (d) and (f). This is because the PCA was so effective to reduce background intensity.

A scatter plot is shown in Fig.7. This was drawn by using the first and second score vectors. Score vectors explains the dispersion of data towards the corresponding eigenvectors [12]. This dispersion shows the difference of spectra, which is called as “principal component score”. As shown in Fig. 7, 2,601 plots obtained from the Fe dried residue were divided into two clusters. Figures 8 (a) and (b) explain the principal component scores of the corresponding spectra shown in the first (t_1) or second (t_2) score vector, respectively. These plots showed cluster 1 and 2 consisted of spectra including Fe peak and other peaks, respectively. According to the above results, it was found that scatter plots were useful to classify and understand spectra obtained by XRF mapping.

Finally, we investigated how PCA was effective for improving the quality of XRF images, regarding the image contrast and spatial resolution. Figure 9(a) shows the Fe Kβ raw image, which is the same as Fig. 5(a). The red rectangle indicates the region where we evaluated the spatial resolution. We longitudinally integrated the XRF intensity in this region. The calculated values were plotted in Fig. 9(b), where the fitted sigmoid curve was also shown. 10 points in blue frame in the left side were analyzed as

background intensities, and other 10 points in green frame in the right side were considered as Fe Kβ intensities. While the standard deviation (SD) for background intensities was 7.31, the SD for Fe Kβ intensities was 8.39. It was found that raw XRF data had a wide dispersion. After the sigmoid curve in Fig. 9(b) was differentiated, the Gaussian curve was obtained as shown in Fig.9(c). FWHM of the differential curve in Fig.9(c) was 32.4 μm, which was considered as a spatial resolution.

Figure 10(a) indicates the Fe Kβ image after PCA as shown in Fig. 5(b). A clear image was shown. The SDs of background intensities and Fe Kβ intensities were smaller than those for raw data, and the more reliable sigmoid curve was obtained in Fig. 10(b). The evaluated differential curve in Fig.10(c) showed a superior spatial resolution, which was 13.9 μm.

Table 1 shows the evaluated SD values for the Fe Kβ and background intensities, obtained for raw data and PCA-filtered data. S-B ratio in Table1 indicates the ratio of the averaged Fe Kβ intensity to the averaged background intensity. Both S-B ratios were almost the same. However, the improvement of SDs for PCA-filtered data led clear constant of XRF images as shown in Fig. 10(a). In addition, the spatial resolution was also improved after PCA as shown in Table 1.

5. Conclusions

We performed XRF mapping for the dried residues. The obtained data matrix-A set was analyzed by PCA, leading to principal components. We recreated PCA-filtered XRF images by using the new data matrix-B, which was made from only principal components. PCA-filtered XRF images were clear with low background intensities, compared to the original raw images. It was also found that improvement of XRF image was effective in the case where the XRF intensity was weak. SDs of XRF intensities in PCA-filtered image were improved, leading to clear contrast of objective image on low background. Also, we confirmed that the spatial resolution in XRF images was improved by applying PCA.

References

[1] N. Gao, K. Janssens, Polycapillary X-ray optics, in: K. Tsuji, J. Injuk, R.E. Van Grieken (Eds.), John Wiley & Sons, Ltd (2004) 293-305.

[2] K. Tsuji, T. Matsuno, Y. Takimoto, M. Yamanashi, N. Kometani, Y. C. Sasaki, T. Hasegawa, S. Kato, Y. Yamada, T. Shoji, N. Kawahara, Spectrochim. Acta Part B, 113 (2015) 43-53.

[3] B. Vekemans, K. Janssens, L. Vincze, A. Aerts, F. Adams and J. Hertogen, X-ray

Spectrom. 26 (1997) 333-346.

[4] Christopher K. Egan, Simon D. M. Jacques and Robert J. Cernik, X-ray Spectrom. 42 (2013) 151–157.

[5] R. Parthasarathy, G. Thiagarajan, X. Yao, Y. P. Wang, P. Spencer, and Y. Wang, J Biomed Opt. 13 (2008) 014-020.

[6] C.R. Appoloni, F.L. Melquiades, Applied Radiation and Isotopes, 85 (2014) 92-95.

[7] K. H. Angeyo, S. Gari, J. M. Mangalab and A. O. Mustaphac, X-Ray Spectrom. 41 (2012) 321–327.

[8] S. Vogt, J. Maser, and C. Jacobsen, J. Phys. IV France, 104 (2003) 617-622.

[9] T. Hasegawa, Anal. Chem., 71 (1999) 3085-3091.

[10] Z. Geng and Q. Zhu, Ind. Eng. Chem. Res, 44 (2005) 3585-3593.

[11] T. Sakabe, S. Yamazaki, and T. Hasegawa, J. Phys. Chem. B, 114 (2010) 6878-6885.

[12] N. Bonnet, Mikrochim. Acta, 120 (1995) 195-210.

Captions

Table 1 Comparison with SD, S-B ratio and spatial resolution.

Figure 1 Experimental setup used micro-XRF measurements for obtaining the elemental map.

Figure 2 Dried residues on glass plate with a volume of 5 ml of 2.5 ppm standard Fe (a) and Cu (b) solutions.

Figure 3 (a) Elemental image created from the spectra obtained by the micro-XRF measurement. (b) Data matrix A (2,601 (spectra) x 2,048 (energy channels). (c) The square matrix created by data matrix A and transposed matrix A^T.(d) Data matrix A resolved into 2,048 eigenvectors and score vectors.

Figure 4 Eigenvalues with different components (the product of eigenvector and score vector).

Figure 5 (a) Micro-XRF image of Fe Kb obtained for the Fe residue (Fig.2(a)), and the PCA-filtered images with (b) 2 components, (c) 10 components, (d) 100 components, (e) 200 components, and (f) 300 components.

Figure 6 (a) Cu Kα image obtained for the Cu residue (Fig.2(b)) with a measurement time of 1s per pixel. Cu Kβ images with different measurement time of 1 s (c) and 10 s (e) per pixel. (b), (d), (f) reconstructed images with PCA-filtered spectra.

Figure 7 Scatter plot by score vector t_1 and t_2, which were obtained from mapping for Fe dried residue.

Figure 8 Principal component scores of the corresponding spectra explained by score vector t_1 (a) and t_2 (b).

Figure 9 (a) Raw Fe Kβ image. (b) Fe Kβ intensity plots. (c) Differential curve.

Figure 10 (a) PCA-filtered Fe Kβ image. (b) Fe Kβ intensity plots. (c) Differential curve.

Table 1 Comparison of SD, S-B ratio and spatial resolution.

	SD for Fe Kβ intensities	SD for BG intensities	S-B ratio	Spatial resolution [μm]
Raw data	**8.39**	**7.31**	**1.92**	**32.4**
PCA-filtered data	**3.46**	**2.31**	**1.85**	**13.9**

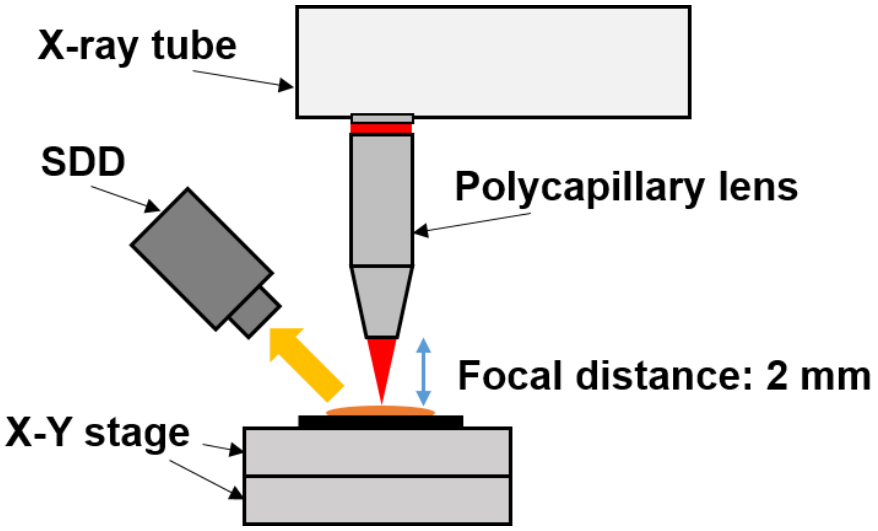

Figure 1 Experimental setup used micro-XRF measurements for obtaining the elemental map.

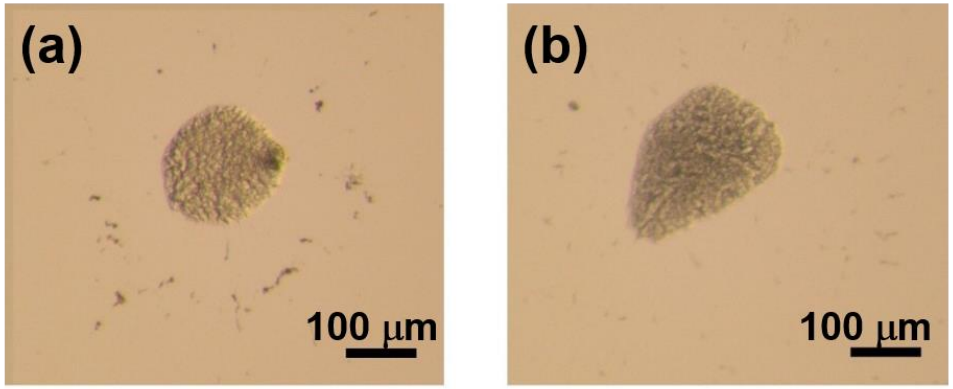

Figure 2 Dried residues on glass plate with a volume of 5 μl of 2.5 ppm standard Fe (a) and Cu (b) solutions.

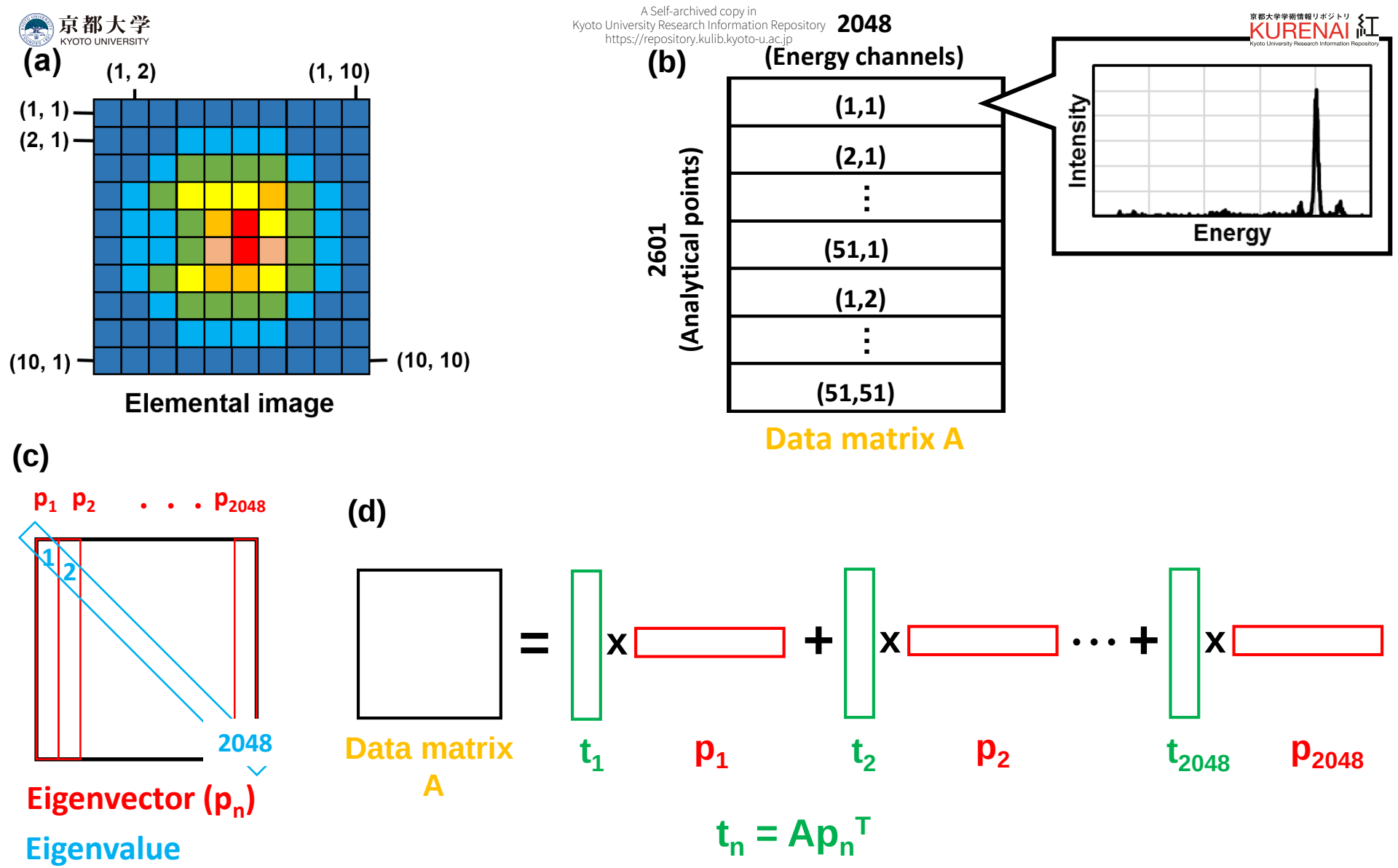

Figure 3 (a) Elemental image created from the spectra obtained by the micro-XRF measurement. (b) Data matrix A (2,601 (spectra) x 2,048 (energy channels). (c) The square matrix created by data matrix A and transposed matrix A^T.(d) Data matrix A resolved into 2,048 eigenvectors and score vectors.

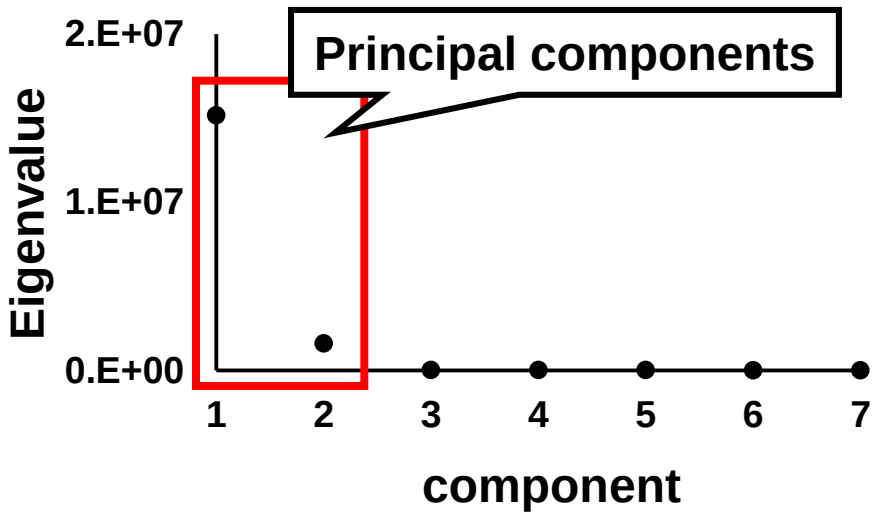

Figure 4 Eigenvalues with different components (the product of eigenvector and score vector).

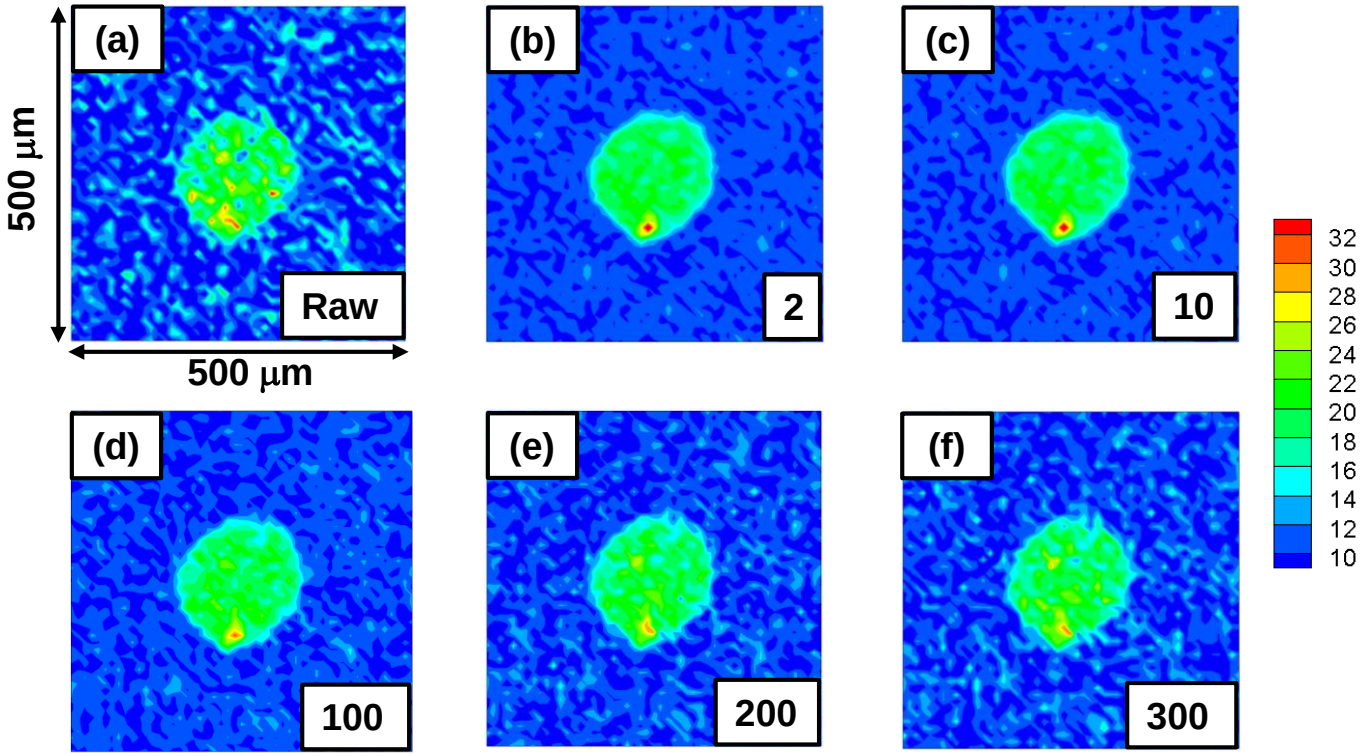

Figure 5 (a) Micro-XRF image of Fe Kβ obtained for the Fe residue (Fig.2(a)), and the PCA-filtered images with (b) 2 components, (c) 10 components, (d) 100 components, (e) 200 components, and (f) 300 components.

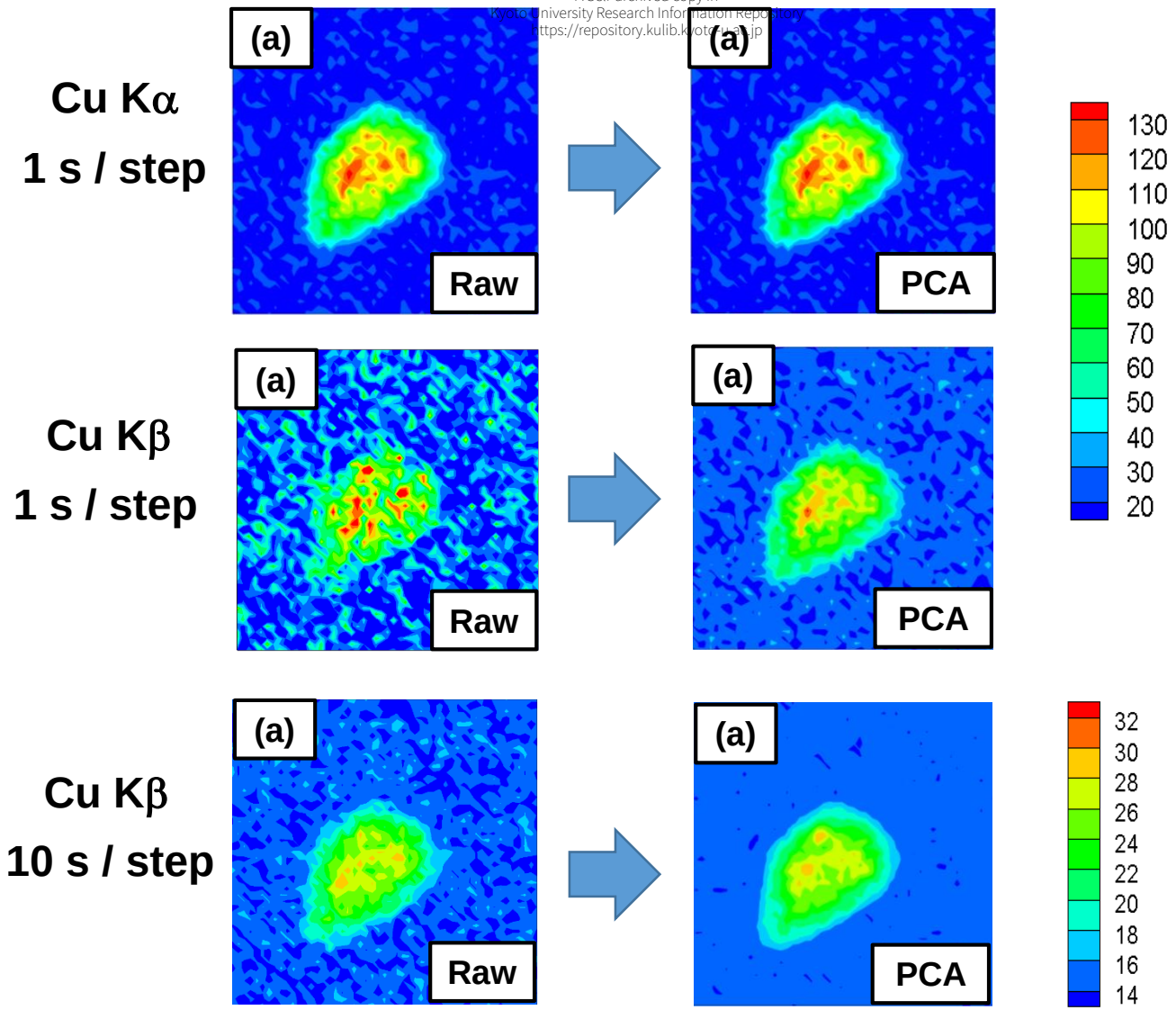

Figure 6 (a) Cu Kα image obtained for the Cu redidue (Fig.2(b)) with a measurement time of 1s per pixel. Cu Kβ images with different measurement time of 1 s (c) and 10 s (e) per pixel. (b), (d), (f) reconstructed images with PCA-filtered spectra.

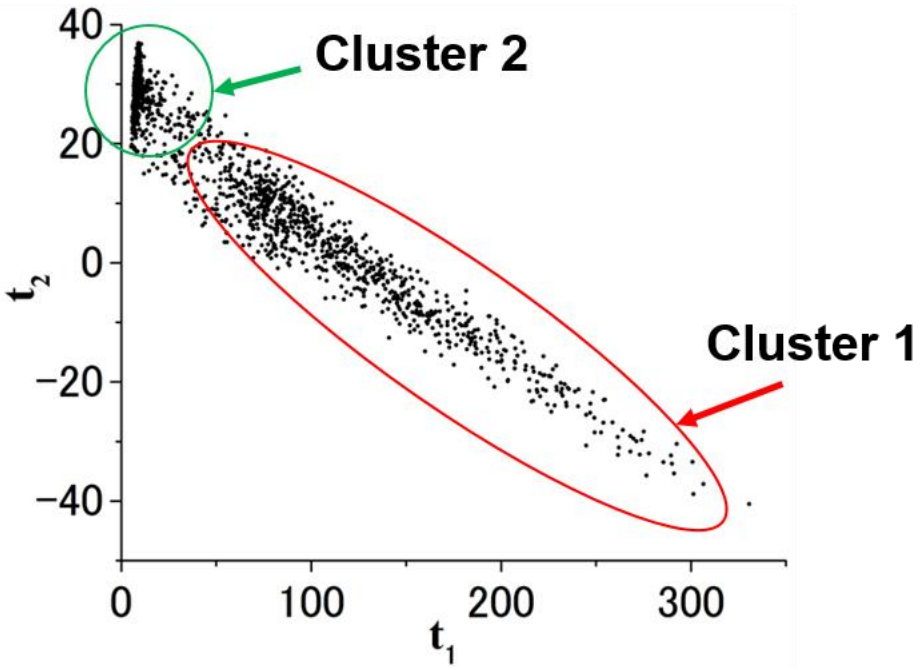

Figure 7 Scatter plot by score vector t_1 and t_2, which were obtained from mapping for Fe dried residue.

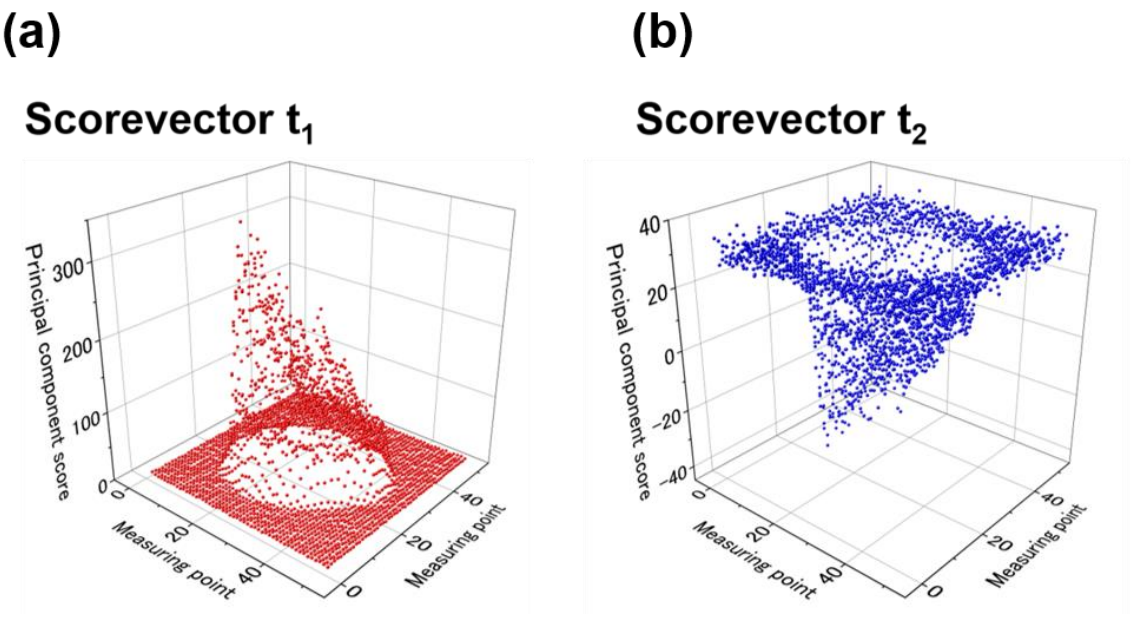

Figure 8 Principal component scores of the corresponding spectra explained by score vector t_1 (a) and t_2 (b).

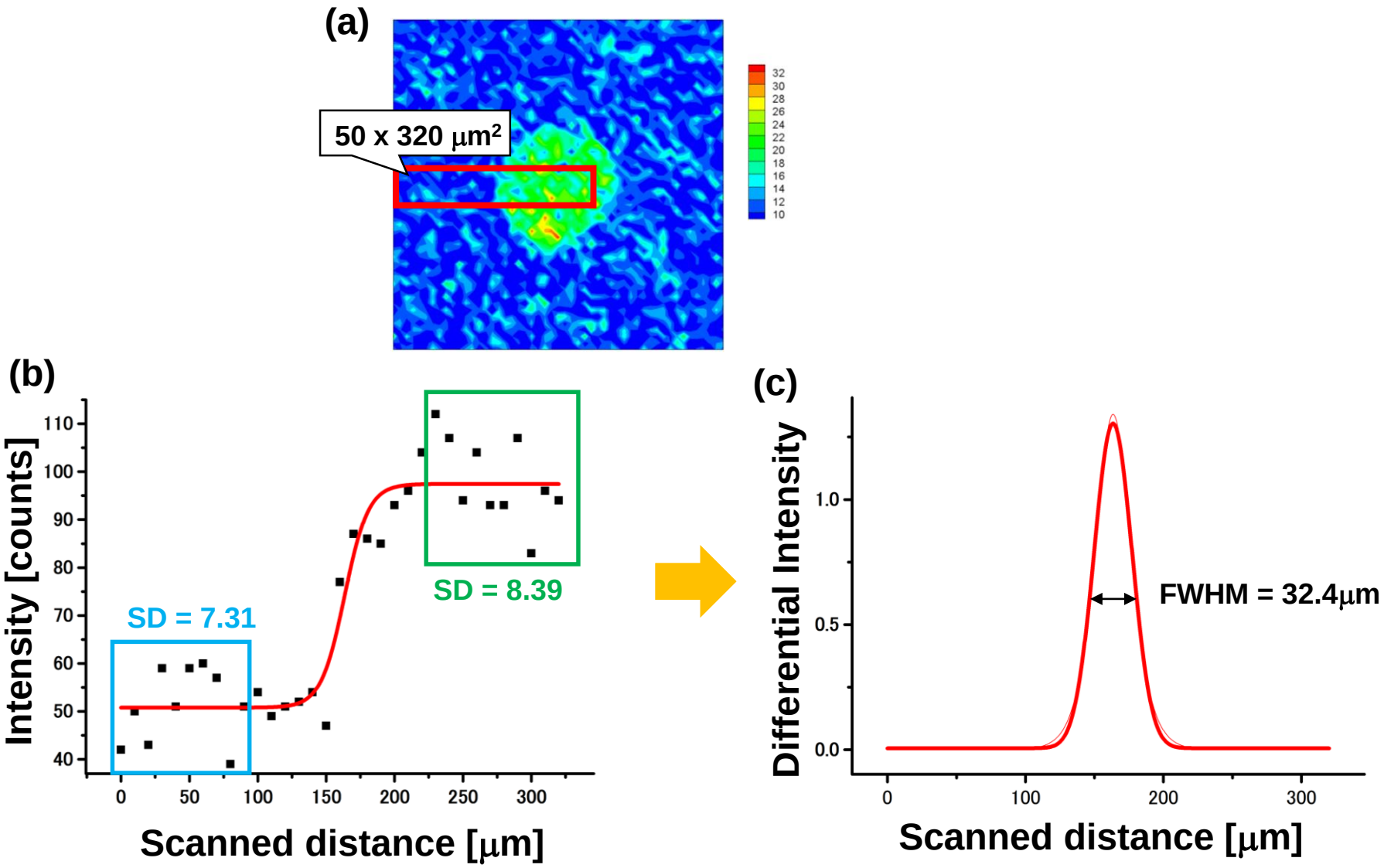

Figure 9 (a) Raw Fe Kβ image. (b) Fe Kβ intensity plots. (c) Differential curve.

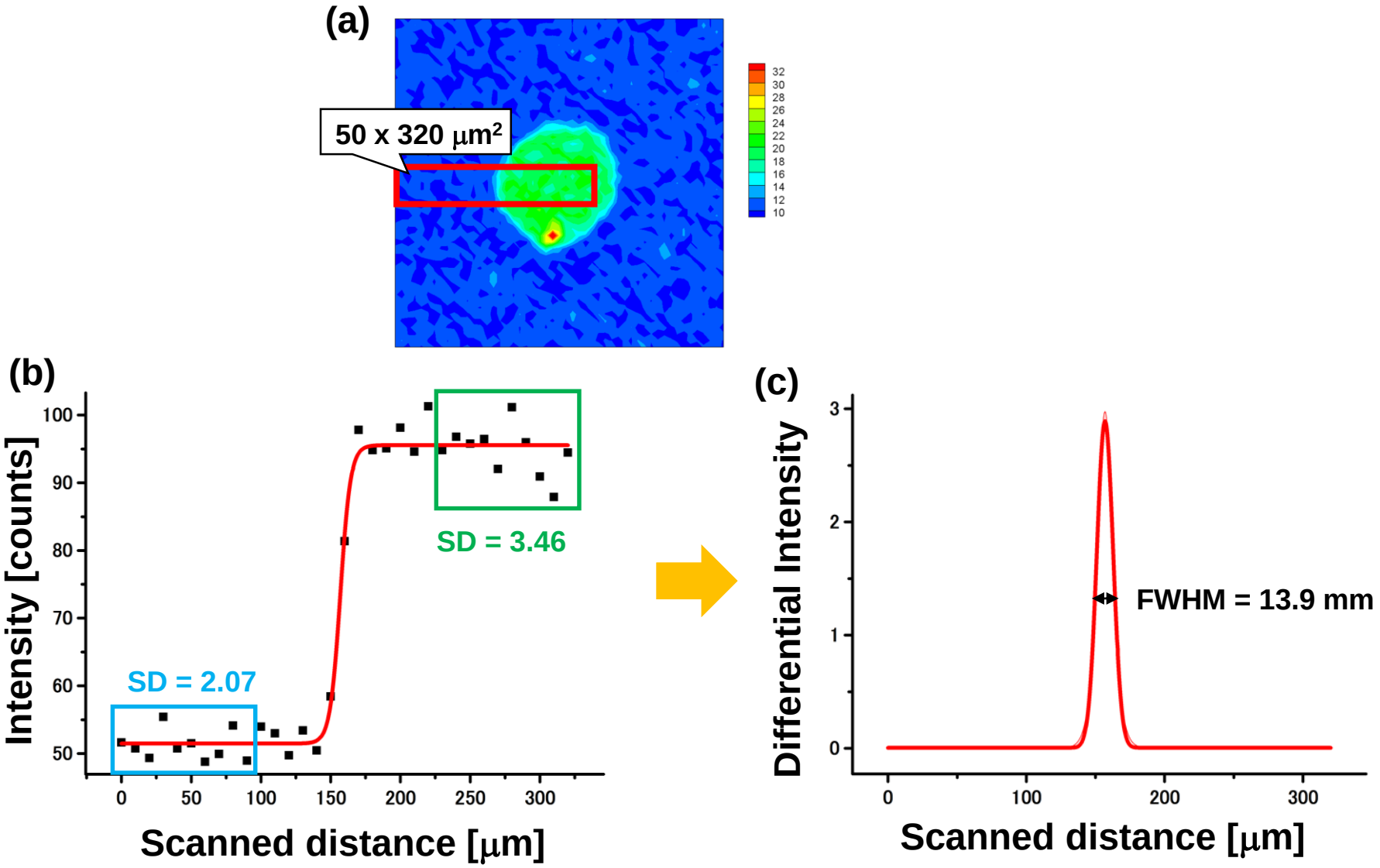

Figure 10 (a) PCA-filtered Fe Kb image. (b) Fe Kb intensity plots. (c) Differential curve.